Sensors and Actuators A: Physical, Volume 397, January 2026, Article number 117233
DOI:10.1016/j.sna.2025.117233

An Ultra-Thin and Lightweight Flexible Actuator for Digitally-Controllable Shape-Morphing Haptics

Yue Chen[a,b], Jian Jiao[b,], Xiaobo Yu[a], Zhen Liu[c,]*, Patrick G. Verdin[d], Zhongqiang Zhang[a,]**

[a] School of Mechanical Engineering, Jiangsu University, Zhenjiang 212013, China

[b] Peng Cheng Laboratory, Shenzhen 518055, China

[c] School of Ship and Ocean Engineering, Jiangsu University of Science and Technology, Zhenjiang 212003, China

[d] Faculty of Engineering and Applied Science, Cranfield University, Cranfield, MK43 0AL, UK

* Corresponding Author. Email: zhangzq@ujs.edu.cn (Z.Q. Zhang); jiaojian2jiaojian@163.com (J. Jiao); liuzhen@just.edu.cn (Z. Liu)

Abstract: With the growing demand for wearable electronics, efficient haptic systems are essential for contact perception and variable haptic feedback. However, achieving a large shape-morphing haptic output is still a challenge for existing flexible robotic actuators. This paper presents a digitally-controllable, ultralight (65 mg), ultrathin (260 μm) flexible actuator that delivers large shape-morphing haptic feedback with an output force of 240 mN and a displacement of 0.88 mm. By integration of micro-circuit printing and micro-fluidic manufacturing technologies, the actuator with significant lightweight and thinness is created. Despite excellent flexibility, the actuator is still able to generate powerful haptic output. User experiments with a haptic signal recognition accuracy of 91.33% validate its potential in wearable devices and human-machine interfaces. Additionally, immersive virtual reality experiments confirmed its ability to recreate realistic tactile sensations, such as perceiving continuous water flow and catching a fast-moving object, highlighting its applicability in embodied intelligence, virtual reality, motion training, and interactive experiences. This study offers new design insights for haptic interfaces in virtual and augmented reality and lays the foundation for future skin-patch-based haptic devices.

Keywords: Haptic feedback; Actuator; Human-machine interaction; Shape-morphing

Published by Elsevier. This is the Author Accepted Manuscript issued with: Creative Commons Attribution License (CC:BY 4.0).
The final published version (version of record) is available online at DOI:10.1016/j.sna.2025.117233. Please refer to any applicable publisher terms of use.

1. Introduction

The human sensory system can capture a vast array of external information, with touch being a critical component that not only connects us closely with our environment and ourselves but also underpins our daily operations and interactions [1-5]. Tactile perception encompasses various sensations, such as temperature, pain, vibration, touch, and pressure, all of which are finely detected by different nerve endings in the skin [6, 7]. The human skin is composed of the epidermis, dermis, and subcutaneous tissue, with the dermis being particularly rich in nerve endings, including tactile corpuscles (Meissner's corpuscles) and pressure receptors (Pacinian corpuscles). These nerve endings are highly sensitive to specific haptic stimuli, allowing us to accurately perceive touch and pressure, which is essential for performing delicate tasks and effectively interacting with our environment in daily life [8-11].

Mechanical vibration, as a well-established haptic feedback technology, is widely utilized in rendering object properties, perceiving interaction positions, and conveying abstract information [12-14]. During human-object interactions, mechanoreceptors can detect a wealth of vibrational information, which, upon processing, allows for the recognition of surface characteristics [15]. For instance, researchers have developed an 18-μm thick dielectric elastomer actuator for wearable haptic feedback devices, capable of generating vibrations in the range of 1 Hz to 500 Hz, enabling users to accurately identify frequency and sequence patterns [16]. Moreover, the 2021 Nobel Prize in Physiology or Medicine was awarded for the discovery of thermoreceptors, laying the foundation for the design of temperature feedback devices. For example, Park et al.[17] developed an advanced skin-integrated system based on thermal perception, which utilizes passive cooling and active thermal control technologies to achieve precise spatiotemporal programming of temperature feedback over extensive areas of the skin, thereby enhancing the human perception of virtual environments. However, these technologies are limited to two-dimensional tactile sensations, lacking the ability to deliver spatial experiences such as thrust or impact, and they do not achieve effective haptic display [18-20].

As a key component of human-machine interaction, haptic display technology is increasingly becoming a vital tool for enhancing user immersion and interaction experiences [21-24]. However, despite the diversity of actuation principles, many existing haptic actuators suffer from large size, heavy weight, and slow response, limiting their suitability for modern applications that demand high wearability, flexibility, and thinness. Moreover, there exist inherent trade-offs among power

efficiency, response speed, durability, and mechanical compliance [25-27]. For instance, while micro-combustion technology provides a highly efficient power source for soft actuators, it faces challenges related to continuous energy supply [28]. Thermoelectric feedback devices [29, 30] provide precise temperature regulation but are constrained by slow response and high energy consumption. Magneto-responsive soft actuators can reproduce programmable surface textures of virtual or remote objects [31]; however, their reliance on bulky magnetic setups inevitably increases system thickness and structural rigidity. Electrohydraulic actuators can produce large displacements and high output forces [32-35]. Nevertheless, their flexibility and adaptability are often compromised by thick or multilayered inextensible polymer shells. Therefore, there is an urgent need to develop ultrathin, lightweight, and highly compliant haptic actuators that can respond rapidly and accurately reproduce complex surface morphologies [36].

This paper presents a digitally-programmable ultra-lightweight (65 mg) and ultra-thin (260 μm) flexible actuator, capable of creating powerful haptic feedback with an output force of 240 mN and a displacement of 0.88 mm. By uniting micro-circuit printing with micro-fluidic manufacturing, the actuator with exceptional lightweight and thinness is fabricated, which has excellent flexibility yet delivers forceful haptic output. User studies demonstrate a haptic signal recognition accuracy of 91.33%, and immersive virtual reality experiments confirm its ability to reproduce realistic tactile experiences, including the perception of continuous water flow and the interaction with rapidly moving objects. Compared with existing technologies, this actuator achieves a unique balance between actuation performance and structural adaptability, offering a promising route toward next-generation skin-conformal haptic systems. These results not only offer new insights into the design of skin-conformal haptic interfaces but also lay the groundwork for future development of high-fidelity, patch-type tactile communication devices.

2. Materials and methods

2.1. Structural design of haptic actuator

The haptic actuator features a multilayer structure, in which a dielectric liquid is encapsulated between two non-stretchable dielectric polymer layers. A stretchable elastic film covers the top active region to enable out-of-plane deformation, while the bottom electrode is insulated and mechanically protected by a layer of polyimide (PI) tape (**Fig. 1a**). This configuration allows the actuator to achieve large, localized displacement under electrical stimulation while maintaining overall mechanical stability and flexibility. To realize the desired ultrathin and lightweight

characteristics, microcircuit printing technology was employed to fabricate high-resolution, ultra-thin silver electrodes. This was paired with microfluidic manufacturing techniques to precisely inject a controlled volume of dielectric oil into the internal cavity. The injection process, enabled by fine-tuned fluidic control, ensures uniform oil distribution and consistent electromechanical response under applied voltage.

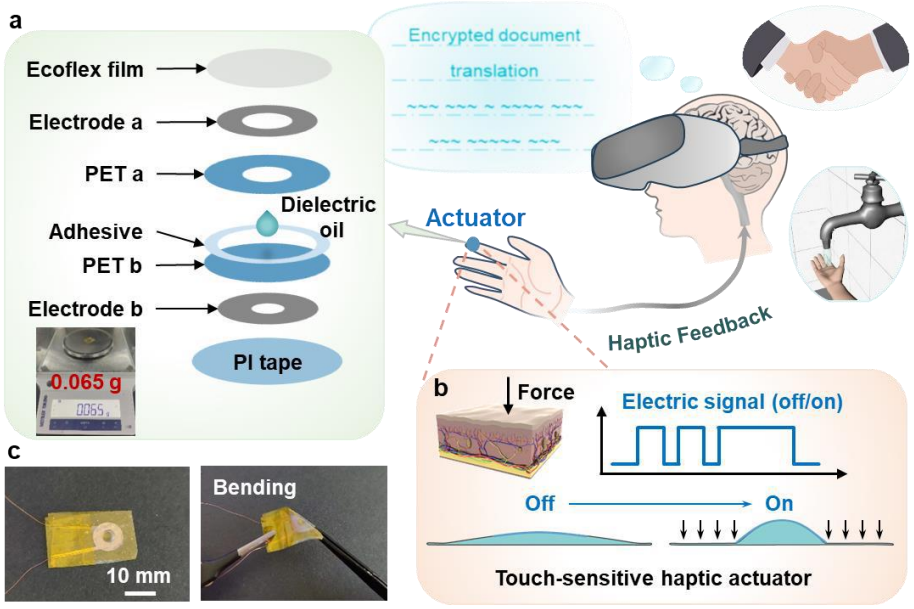


Fig. 1 Application and structure of the haptic actuator. (a) The composition of the haptic actuator. (b) Signal transmission via the on/off state of the voltage-driven actuator. (c) Photograph of the actual haptic actuator.

The actuation system consists of a personal computer that wirelessly transmits control commands via Bluetooth to a portable high-voltage power supply (as illustrated in **Fig. S1**). The power supply delivers voltage signals to the actuator, inducing deformation through electrohydraulic expansion. When in contact with the human body, the actuator transmits perceivable tactile cues by modulating the voltage input, enabling interactive haptic feedback (as depicted in **Fig. 1b**). This system design supports applications in immersive virtual environments and wearable human-machine interfaces. To further investigate and optimize the working principles of the actuator, numerical simulations were conducted based on its multilayer geometry and material properties to analyze voltage-induced deformation behavior. The simulation results provided valuable guidance for structural optimization and were further validated through experimental measurements. Compared with existing haptic technologies, the actuator exhibits a significantly reduced thickness and weight, while maintaining excellent flexibility and tactile

display capabilities (see **Fig. 1c**). These features make it highly suitable for a range of interactive applications, such as replicating the sensation of a handshake or perceiving dynamic virtual forces.

2.2. Fabrication processes of haptic actuator

The fabrication process of five haptic actuators with varying aperture sizes (see Supplementary **Fig. S2**) is illustrated in **Fig. 2**. First, the polyethylene terephthalate (PET) film (thickness: 5 μm), which serves as the dielectric polymer layer, underwent pre-treatment. The surface of the PET film was activated using a plasma device. Subsequently, silver electrodes were printed onto the activated PET film using a microcircuit printer. After printing, the PET film was dried in an oven at 100 ℃ for 2 h. The PET film with printed silver electrodes was then cut using a laser cutter, based on the electrode positions.

Next, the assembly of the film layers was carried out. An elastic film (Ecoflex 00-30, Smooth-On Inc) was first adhered and laminated over the notched electrodes using silicone adhesive (Sil-Poxy, Smooth-on Inc.). After the adhesive cures, the PET film with silver electrodes was adhered to the side of the elastic film that remains uncovered. The adhesive was applied evenly around the electrodes in a thin layer, with a coating thickness of approximately 5 μm.

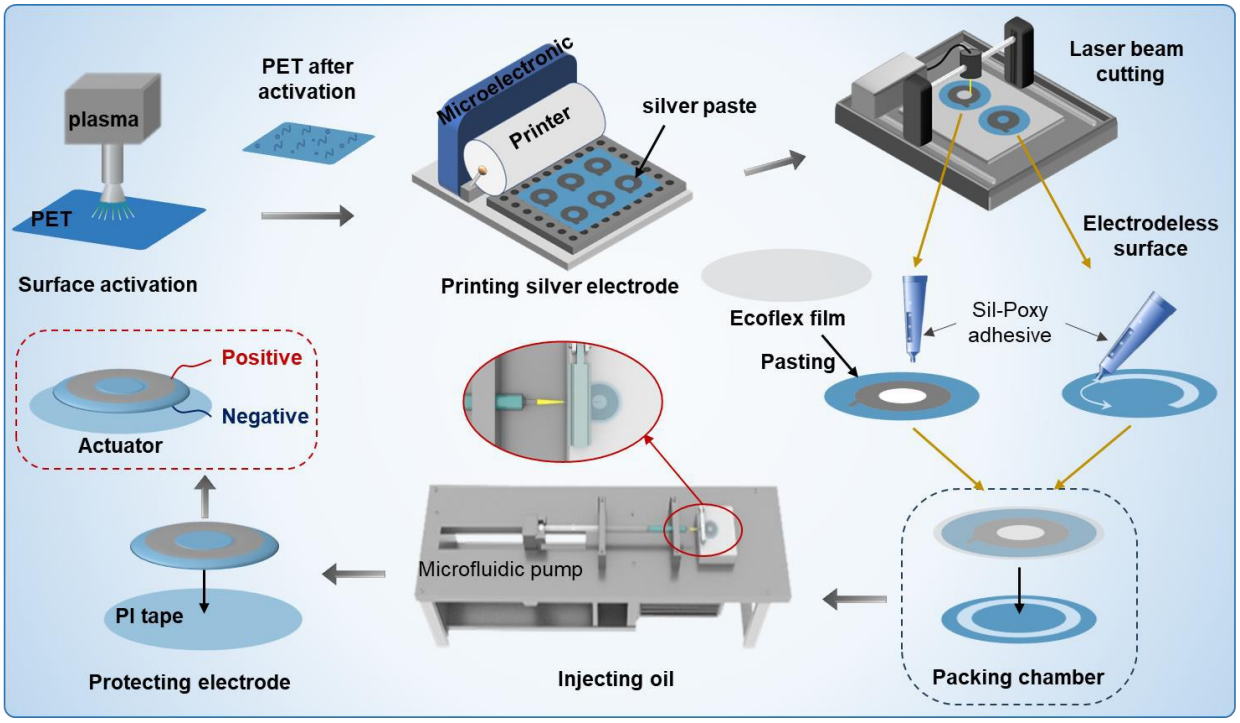


Fig. 2 Schematic of the fabrication process for the haptic actuator.

To accurately control the dielectric oil injection volume, we developed a set of custom-designed microfluidic system. A precise amount of the dielectric oil (Envirotemp FR3, Cargill Inc.) was injected between the layers using the microfluidic system before the adhesive between the PET layers fully cures. The exposed electrodes were then sealed with polyimide (PI) tape, completing the fabrication of the haptic actuator.

2.3. Methods

The silver electrodes were printed on PET using a microcircuit printer (DP500, BroadTeko) with nanosilver ink (BroadCON-INK550, BroadTeko), and the PET was cut using a laser cutter. A uniaxial load cell (DSZ-100, Decent Inc.) was employed to measure the force and a laser displacement sensor (HL-G103-S-J, Panasonic Inc.) was used to measure the displacement. Additionally, a high-speed camera (VEO 710, Phantom, USA) was utilized to capture real-time images of the experiment.

3. Results and discussion

3.1. Model design

The model of haptic actuator was subjected to an analytical study based on the Computational Fluid Dynamics (CFD) Module, the Structural Mechanics Module, and the AC/DC Module within the finite element modelling (FEM) software COMSOL Multiphysics suite [37]. The model of the haptic actuator, as depicted in **Fig. 3a**, was derived from a two-dimensional axisymmetric model through rotational transformation (see Supplementary **Fig. S3**). During the simulation process, a transient analysis was conducted under two distinct conditions: (1) The motion state of the top Ecoflex layer was analyzed to ascertain the maximum displacement. (2) A rigid slab was introduced directly above the model, and an integration was performed at the designated red boundary (as illustrated in Supplementary **Fig. S4**) to document the variation in exerted force. Through these two transient analyses, we comprehensively evaluated the physical behavior of the haptic actuator under different operating conditions, providing critical data to support further design optimization and performance enhancement.

3.2. Working principle

The working principle of the haptic actuator involves injecting dielectric oil into a pouch made of dielectric polymer, with silver electrodes printed on both sides of the pouch. Notably, one side of the electrode has a circular aperture covered by a layer of elastic film. When a voltage is applied, the electrodes on both sides attract each other, generating electrostatic Maxwell stress that acts on

the dielectric oil inside the pouch [33]. As the edges of the electrodes move towards the central region, resembling a zipper closure (the mesh deformation process of the haptic actuator during this process is shown in **Fig. 3b**) [38], the dielectric oil is squeezed into the central gap (see **Video 1**). The hydraulic pressure generated during this process causes the elastic film covering the aperture to deform (**Fig. 3c)** illustrates the displacement model of the cross-section of the haptic actuator). By adjusting the applied voltage, the stress-strain response of the haptic actuator can be precisely controlled [34]. The electrostatic pressure generated on the electrodes of the haptic actuator is given by:

$$P = \frac{1}{2}\varepsilon_0 \varepsilon_r E^2, \tag{1}$$

where ε_r and ε_0 are the dielectric constants of the dielectric oil and vacuum, respectively. The electrodes of the haptic actuator can be approximated as a non-parallel plate capacitor (as shown in the inset below **Fig. 3c**), with the extension lines of the two plates intersecting at angle θ at point O. Assuming the distance from any point between the plates to point O is r, with σ the charge density on the electrodes, the electric field strength between the two electrodes is:

$$E = \frac{\sigma\left(R_2 - R_1\right)}{\varepsilon\varepsilon_0 r \ln\dfrac{R_2}{R_1}}. \tag{2}$$

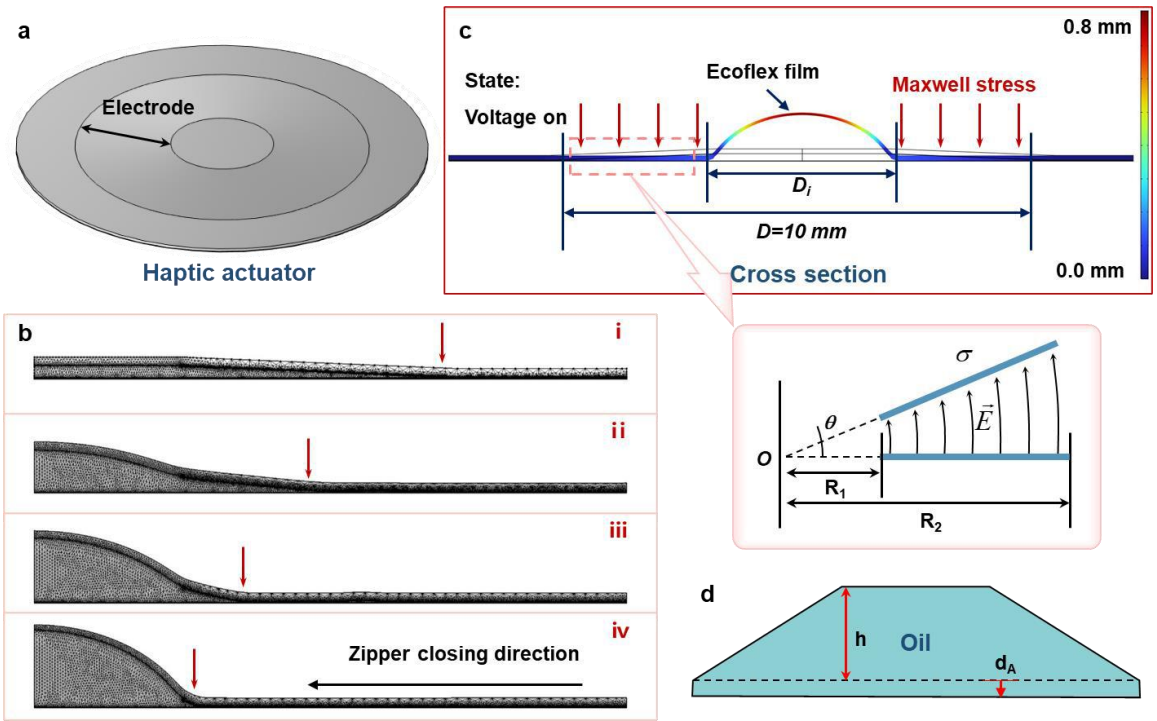


Fig. 3. (a) 3D simulation model of the haptic actuator. (b) Mesh deformation of the actuator when voltage is applied. (c) Displacement model of the cross-section of the haptic actuator and electrode analysis model. (d) Schematic diagram of the cross-section of the dielectric oil.

Considering the incompressibility of the dielectric oil, the volume V of the haptic actuator remains constant before and after the voltage is applied. Therefore, when the electrodes are fully closed, the top displacement L of the haptic actuator can be predicted. When no voltage is applied, the dielectric oil inside the haptic actuator can be approximated as the volume of a frustum of a cone combined with that of a cylinder (as shown in **Fig. 3d**):

$$V = \frac{1}{12}\pi h\left(D_i^2 + D^2 + D_i D\right) + \frac{1}{4}\pi d_A D^2, \tag{3}$$

where h and d_A are the heights of the frustum and cylinder respectively, D is the electrode diameter, and D_i is the diameter of the hole. When the electrodes are fully closed, the dielectric oil inside the haptic actuator can be approximated as half an ellipsoid:

$$V = \frac{1}{6}\pi H D_i^2, \tag{4}$$

where H is the height of the ellipsoid. From this, the top displacement L of the haptic actuator can be obtained, following $L = H - h - d_A$.

3.3. Validation of haptic actuator

This study investigates the output normal force and displacement of different aperture haptic actuators. Prior to practical testing, a simulation model was established using COMSOL (illustrated in **Figs. 4a** and **b**) to explore the effects of model design and voltage on the force and displacement of the haptic actuators, thus optimizing their structure [39]. Initially, the impact of the membrane thickness on the performance of the haptic actuators was examined. Since PET acts as a dielectric between the electrodes, a thinner PET film requires lower voltage, leading to a focus on the thickness of the stretchable elastic membrane (Ecoflex 00-30). The simulation results (Supplementary **Figs. S5a** and **b**) indicate that as the thickness of the elastic membrane decreases, the displacement increases. This is because a thinner elastic membrane requires less resistance to its restoring force, achieving a maximum displacement of 0.82 mm at a thickness of 70 μm and a voltage of 2530 V, beyond which the displacement no longer increases. However, if the elastic membrane is too thin, its rigidity decreases, adversely affecting force transmission. Consequently, at higher voltages (2700-3000 V), the force exerted by a 70 μm thick elastic membrane diminishes.

Therefore, in subsequent model optimization and testing experiments, a 100 μm thick Ecoflex 00-30 membrane was considered.

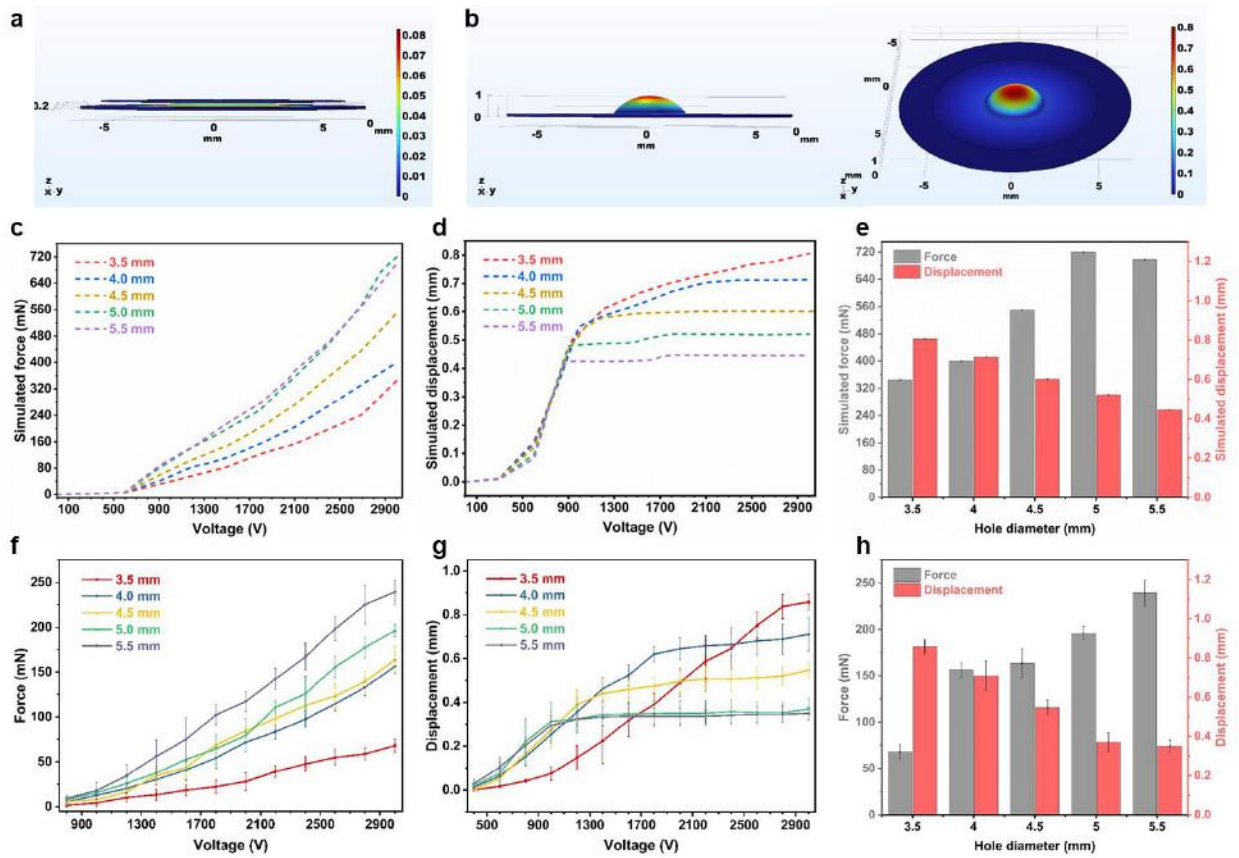


Fig. 4. Measured and simulated force and displacement of haptic actuators with different aperture designs. (a) and (b) Model simulations of the haptic actuator's force and displacement. (c) and (d) Simulated force and displacement of the haptic actuator as a curve of voltage. (e) Summary of the simulated force and displacement of the haptic actuator at 3000 V. (f) and (g) Measured force and displacement of the haptic actuator as a curve of voltage. (h) Summary of the measured force and displacement of the haptic actuator at 3000 V.

Simulation results (depicted in **Fig. 4c**) indicate that the force generated by the haptic actuator increases with rising voltage, and a larger aperture results in a greater force output. The maximum output was achieved with apertures ranging from 5.0 to 5.5 mm. As the aperture increases, a greater volume of dielectric fluid rapidly enters the elastic region of the actuator, enhancing the volume of the dielectric medium within this region and thereby increasing the force produced [32]. However, beyond a certain point, further increases in aperture size lead to a reduction in force (see Supplementary **Fig. S6**). An excessively large aperture may prevent the dielectric fluid from being

effectively confined within the actuator, which could reduce the compressive force generated under the electric field, ultimately leading to a decrease in output force.

The simulation results regarding the displacement of the haptic actuator are shown in **Fig. 4d**. When the voltage reaches 900 V, it results in a very slow increase in displacement as the electrodes approach full closure. Displacement decreases as the aperture increases, aligning with **eq. (5)**, which states that a larger diameter at the base of the semi-ellipse results in a smaller height *L*. In summary, within the aperture range of 3.5 to 5.5 mm (as presented in **Fig. 4e**, which consolidates the force and displacement of haptic actuators with various apertures at 3000 V), the simulated force and displacement of the haptic actuator increase and decrease, respectively, with increasing aperture size.

To validate the experiments, a portable 150 Hz square wave power supply was used to provide voltage to the haptic actuators, allowing us to investigate the impact of voltage on actuator behavior. Under voltage drive, the haptic actuators exhibited zipper-like motion due to electrostatic pressure, rapidly forcing the dielectric liquid into the elastic region (as shown in the comparison photos before and after voltage application in Supplementary **Fig. S7**). Haptic actuators can function as a haptic display device, clearly illustrating the changes in the actuator's protrusion [40]. The displacement curve of the haptic actuators over time (as illustrated in Supplementary **Fig. S8**) indicates a rapid response, with the actuator transitioning from powered on to electrode closure in just 0.6 s.

In the force testing, different preload conditions were considered, as they could affect the internal stress distribution within the actuator and, consequently, the force output [41]. For the haptic actuator with a 5.5 mm aperture, the force output was systematically studied under various preload conditions at 3000 V (see Supplementary **Fig. S9**). The results indicate that the force increases with preload and reaches a plateau around 12 mN. Therefore, a preload of 12 mN was employed in subsequent force tests. The experimental results showed strong agreement with simulation predictions (as depicted in **Fig. 4f** and **g**). The testing forces and displacements at different apertures under 3000 V are plotted in Fig. 4h, where the maximum normal force of 240 mN was achieved with a 5.5 mm aperture, and the maximum displacement of 0.88 mm was observed with a 3.5 mm aperture. These values are well above the human tactile perception threshold, indicating the actuator can provide perceivable fingertip-scale haptic feedback.

Furthermore, to explore the dynamic electromechanical behavior, additional experiments were conducted to measure the output force of a 4.0 mm aperture actuator under a constant square-wave driving voltage of 3000 V, with frequencies ranging from 10 Hz to 150 Hz in increments of 10 Hz. As shown in Supplementary **Fig. S10**, the output force gradually decreased with increasing frequency. At lower frequencies (10-30 Hz), the actuator exhibited relatively high output forces of approximately 165-190 mN, while the output force monotonically decreased and stabilized around 158 mN at 150 Hz. This behavior indicates that lower frequencies favor larger deformation amplitudes and stronger output forces, making them suitable for quasi-static or continuous tactile feedback (e.g., surface texture perception), whereas higher frequencies facilitate rapid vibration responses ideal for transient or impact-like tactile sensations.

3.4. User evaluation

To demonstrate the potential of the haptic actuator in wireless password information transmission, we conducted a digital recognition test [42]. **Fig. 5a** depicts a scenario where a participant uses the haptic actuator device in front of a personal computer (PC). The participant wears the haptic actuator on the tip of one finger while operating the computer mouse with the other hand. The device is powered by a rechargeable portable power supply that provides voltage signals and receives instructions from the PC via a Bluetooth receiver. The digits 0-9 on the PC interface correspond to different schematic diagrams (as shown in **Fig. 5b**). Each digit is represented by voltage signals of varying durations, with long signals (3 s) depicted as long lines and short signals (1 s) as dots (**Fig. 5c**). For example, the digit 3 is generated by a sequence of voltage signals consisting of 1, 3, and 1 s, with a 0.5 s interval between each signal. Specifically, a single short signal represents the digit “9,” while a single long signal represents “0.” Digits 1-8 are encoded by combinations of three long and short signals following a binary-like pattern, as illustrated in **Fig. S11**. This encoding scheme enables participants to associate each tactile pattern with a specific number during the test. The corresponding signal patterns of each digit are clearly displayed on the PC testing interface, allowing participants to accurately interpret the tactile information.

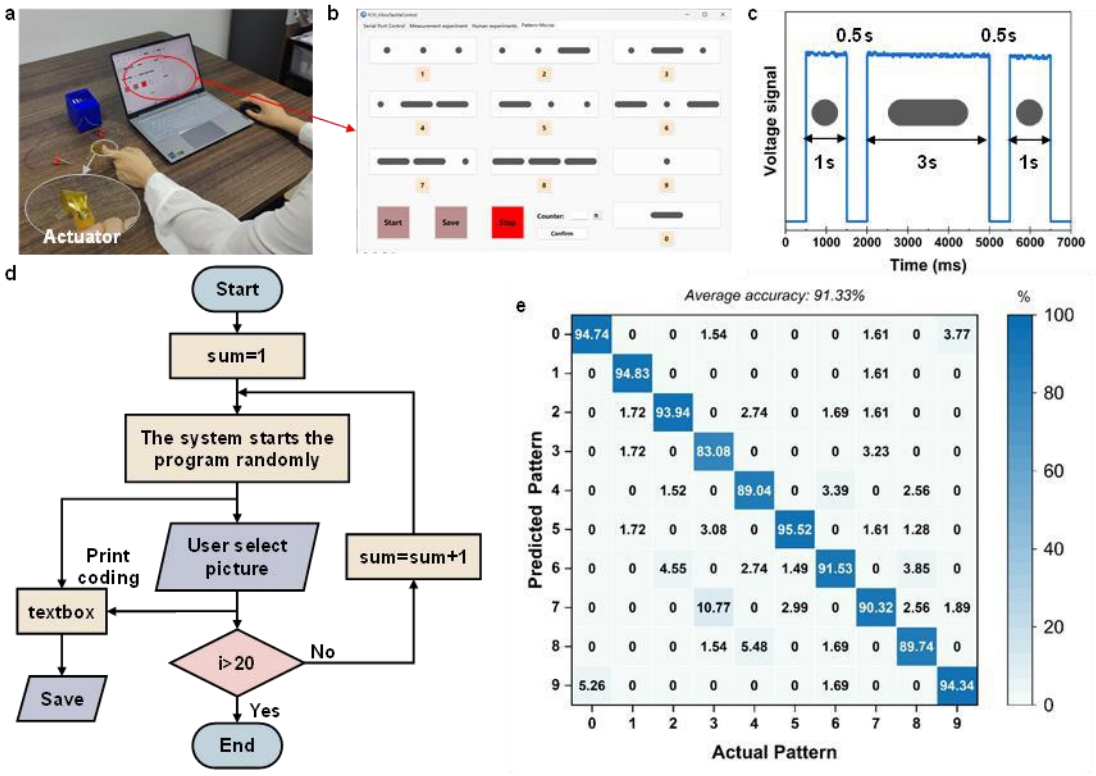


Fig. 5. (a) Photograph of a participant recognizing and reading the haptic actuator signals. (b) Test window displayed on the personal computer (PC). (c) Schematic diagram of the voltage signal corresponding to the digit "3", with the haptic actuator activated at a 2200 V driving voltage. (d) Flowchart of the password testing procedure: The system automatically records and saves each voltage signal and the user's selected image, and the program stops after 20 selections. (e) Confusion matrix results of participant password test.

When the participant clicks the "Start" button, the system randomly generates a voltage signal representing a digit from 0 to 9. The participant then selects the corresponding image based on the information perceived through their fingertip. Following this, the system generates another voltage signal, and the participant completes 20 judgments per test session, with each participant participating in three sessions (the test procedure is illustrated in **Fig. 5d**). To mitigate potential numbness and mental fatigue caused by prolonged fingertip vibrations and decision-making, participants were given a 5-min break after each session. A total of 10 participants participated in this experiment, resulting in 600 sets of data. The experimental results are summarized in the confusion matrix shown in **Fig. 5e**, with an average recognition accuracy of 91.33 %. This experiment demonstrates the feasibility of encoding and transmitting digital information through tactile stimuli, suggesting potential applications of the proposed haptic actuator in secure information encryption within the field of haptics.

To demonstrate the role of an ultra-lightweight and ultra-thin haptic interface in enhancing interaction with the virtual world, an immersive VR application is presented (**Fig. 6a**). When the user clicks the play video button, the host computer receives the playback signal and transmits a command via Bluetooth to the power control center. The control center then forwards the command to the haptic actuator, which generates the corresponding haptic feedback, enabling the user to perceive diverse virtual tactile experiences. **Video 2** further demonstrates the potential application of the haptic actuator in virtual interactions. The fabricated haptic actuator, characterized by its flexibility and ultra-thin lightweight design, can be attached to various parts of the human body without causing additional burden to the wearer. Additionally, the use of a portable power supply ensures device safety, preventing any pulling sensation during wear while also eliminating concerns about electric shock, thereby improving overall comfort.

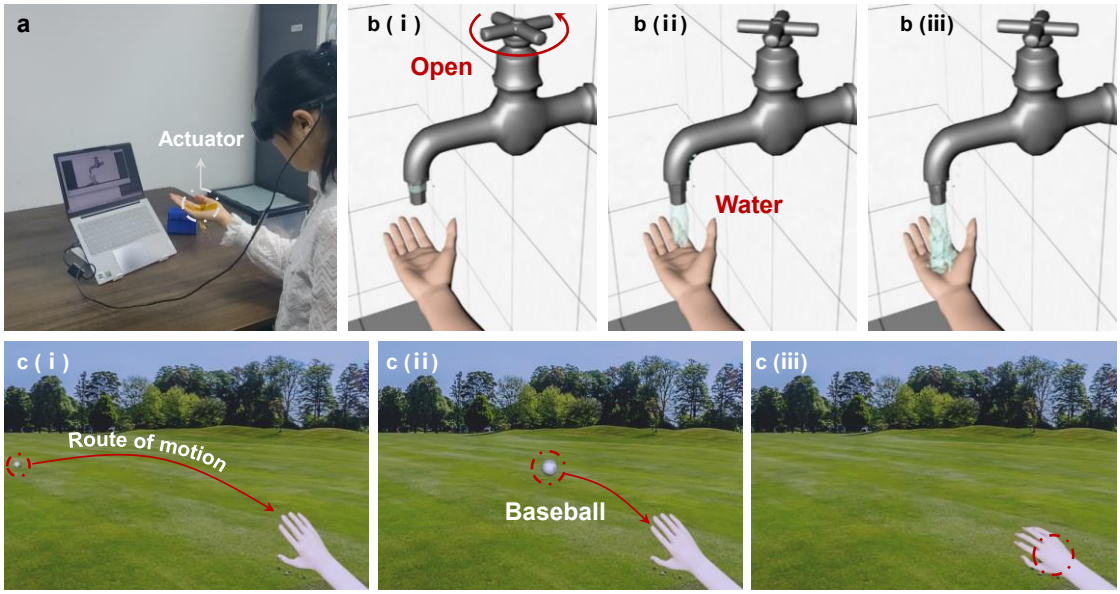


Fig. 6. (a) Schematic diagram of a user wearing VR glasses for visual feedback. (b) Simulated sensation of continuous water flow striking the palm under 2200 V voltage and 20 Hz frequency. (c) Simulated sensation of catching a fast-approaching baseball under 2200 V voltage and 150 Hz frequency.

In the experimental demonstration, volunteers wore the haptic actuator and experienced two representative haptic interaction scenarios in the virtual environment: (1) sensing the flow of water from a faucet on the palm (**Fig. 6b**) and (2) catching a fast-approaching baseball with the palm (**Fig. 6c**). During these interactions, the haptic actuator generated corresponding tactile feedback based on the distinct physical properties of the virtual objects, enhancing the user's immersive experience. According to the response characteristics of cutaneous mechanoreceptors, frequencies of 20 Hz and 150 Hz were selected for the two scenarios, respectively: 20 Hz primarily stimulates

Meissner corpuscles, which respond to low-frequency vibrations and are associated with continuous sensations such as flowing water, whereas 150 Hz activates Pacinian corpuscles, which are sensitive to high-frequency vibrations and correspond to transient impact sensations, such as catching a moving baseball. These frequency selections and the corresponding vibration responses are consistent with the experimental results shown in Supplementary **Fig. S10**.

To further assess the actuator's reliability under long-term operation, cyclic impact and fatigue tests were conducted (**Fig. S12**). The actuator with a 5.5 mm aperture was fixed onto a rigid holder using PI tape, while the probe of a digital force gauge was fitted with a hemispherical silicone pad to simulate fingertip contact conditions. Under the control of a single-axis motion stage, the actuator was subjected to 1000 repetitive impact cycles under a 0.5 N load. Throughout the entire testing process, the actuator maintained its structural integrity without visible damage or fluid leakage, demonstrating excellent mechanical robustness and fatigue resistance. Moreover, the output force and displacement remained stable at around 140 mN and 0.33 mm, showing no evident degradation after 1000 cycles (**Fig. S13**). These results confirm the actuator's long-term operational stability and structural reliability for repeated wearable haptic interactions.

Furthermore, **Fig. 6(i)**, **(ii)**, and **(iii)** depict key frames of the virtual interaction process: the initial state, the interaction phase (where the palm gradually approaches the virtual object), and the final state (when the palm makes full contact with the target object). These experimental results demonstrate that the designed ultra-thin haptic actuator effectively enhances tactile immersion in VR environments, providing valuable insights for the future application of wearable haptic technology in human-machine interaction.

4. Conclusion

In summary, this paper reports a digitally-controllable, ultra-lightweight, ultra-thin flexible actuator that delivers large shape-morphing haptics with powerful output force. By combining micro-circuit printing with a custom-designed micro-fluidic system, the actuator that is dramatically thin and lightweight is fabricated, yet retain exceptional flexibility while creating large haptic feedback.

The actuator consists of a dielectric liquid encapsulated between a non-stretchable dielectric polymer layer and a stretchable elastic film, allowing efficient voltage-induced deformation and tactile signal transmission. Numerical analysis provided a theoretical basis for geometric optimization, and experimental validation confirmed its high output force (240 mN) and

displacement (0.88 mm). A signal recognition accuracy of 91.33% further demonstrates its potential as a portable and silent haptic information transmission system. In addition to functioning as a tactile encoder for pattern recognition, the actuator effectively recreated realistic sensations such as flowing water and dynamic impacts in immersive virtual reality scenarios. These results underscore its potential in wearable electronics, virtual environments, robot teleoperation, and human-machine interaction. This work contributes to the development of high-performance, skin-conformal haptic systems capable of enhancing interactive experiences.

CRediT authorship contribution statement

Yue Chen: Writing - original draft, Methodology, Investigation, Formal analysis, Data curation, Conceptualization. **Jian Jiao:** Writing - review & editing, Project administration, Methodology, Funding acquisition, Formal analysis. **Xiaobo Yu:** Investigation, Data curation, Methodology. **Zhen Liu:** Writing - review & editing, Supervision, Project administration, Formal analysis. **Patrick G. Verdin:** Writing - review & editing, Formal analysis. **Zhongqiang Zhang:** Writing - review & editing, Supervision, Project administration, Investigation, Funding acquisition, Formal analysis, Conceptualization.

Declaration of competing interest

The authors declare that they have no known competing financial interests or personal relationships that could have appeared to influence the work reported in this paper.

Acknowledgements

This work was supported by the Frontier Technologies R&D Program of Jiangsu (BF2024047), the Major Program of NSFC for Basic Theory and Key Technology of Tri-Co Robots (92248301), the Major Key Projects of PCL under Grants (PCL2025A12-2, PCL2024A04-1), the Guangdong S&T Programme under Grant (2024B0101010003), and the postgraduate research & practice innovation program of Jiangsu province (KYCX22_3617).

Appendix A. Supporting information

Supplementary data associated with this article can be found in the online version at DOI.

References

[1] M.W.M. Tan, H. Wang, D. Gao, P. Huang, P.S. Lee, Towards high performance and durable soft tactile actuators, Chem. Soc. Rev., 53(2024) 3485-535. https://doi.org/10.1039/d3cs01017a.
[2] Y.y. Luo, C. Liu, Y.J. Lee, J. DelPreto, K. Wu, M. Foshey, et al., Adaptive tactile interaction transfer via digitally embroidered smart gloves, Nat. Commun., 15(2024) 868. https://doi.org/10.1038/s41467-024-45059-8.
[3] W. Ji, G.z. He, B. Xu, H. Zhang, X. Yu, A new picking pattern of a flexible three-fingered end-effector for apple harvesting robot, Agriculture, 14(2024) 102. https://doi.org/10.3390/agriculture14010102.
[4] K.-H. Ha, J. Yoo, S. Li, Y.x. Mao, S.w. Xu, H.y. Qi, et al., Full freedom-of-motion actuators as advanced haptic interfaces, Science, 387(2025) 1383-90. https://doi.org/10.1126/science.adt2481.
[5] D. Zhao, J. Shan, S. Ding, D. Fang, S. Liu, K. Zhang, et al., Spatiotemporal rendering for dynamic sensation reproduction via electrostatic-enhanced vibro-haptic interface, The Innovation, 6(2025) 101035. https://doi.org/10.1016/j.xinn.2025.101035.
[6] L.L. Becerra, N.B. Root, R.S. Ramji, R. Rouw, D.J. Lipomi, Use of Materials Science to Understand Haptic Perception, Acc. Mater. Res., 6(2024) 136-46. https://doi.org/10.1021/accountsmr.4c00207.
[7] A.D. André, I. Coondoo, I. Bdikin, V.K. K.B, R.M.R. Pinto, P. Martins, et al., Piezo-ionic actuator for haptic feedback, Sens. Actuators A: Phys., 381(2025) 116038. https://doi.org/10.1016/j.sna.2024.116038.
[8] Y.t. Gong, K.j. Zhang, I.M. Lei, Y. Wang, J. Zhong, Advances in piezoelectret materials-based bidirectional haptic communication devices, Adv. Mater., 36(2024) 2405308. https://doi.org/10.1002/adma.202405308.
[9] Y.h. Zhou, X. Zhao, J. Xu, G. Chen, T. Tat, J. Li, et al., A multimodal magnetoelastic artificial skin for underwater haptic sensing, Sci. Adv., 10(2024) eadj8567. https://doi.org/10.1126/sciadv.adj8567.
[10] Y. Huang, J.k. Zhou, P.c. Ke, X. Guo, C.K. Yiu, K.m. Yao, et al., A skin-integrated multimodal haptic interface for immersive tactile feedback, Nat. Electron., 6(2023) 1020-31. https://doi.org/10.1038/s41928-023-01074-z.
[11] J.z. Liu, J. Liang, S.y. Zhao, Y.x. Jiang, J. Wang, Y.c. Jin, Design of a virtual multi-interaction operation system for hand-eye coordination of grape harvesting robots, Agronomy, 13(2023) 829. https://doi.org/10.3390/agronomy13030829.
[12] J.H. Kim, A. Vazquez-Guardado, H. Luan, J.T. Kim, D.S. Yang, H. Zhang, et al., A wirelessly programmable, skin-integrated thermo-haptic stimulator system for virtual reality, Proc. Natl. Acad. Sci. U.S.A., 121(2024) e2404007121. https://doi.org/10.1073/pnas.2404007121.
[13] Z. Ma, Z.l. Zhang, Z.h. Zhang, Z.q. Song, Y.b. Liu, Y.m. Li, et al., Durable testing and analysis of a cleaning sieve based on vibration and strain signals, Agriculture, 13(2023) 2232. https://doi.org/10.3390/agriculture13122232.
[14] C. Zhang, M. Li, Z. Wu, C.-G. Zhao, H. Yuan, J. Xie, et al., A haptic feedback sleeve for a flight video game, IEEE Trans. Haptic, 18(2025) 198-207. https://doi.org/10.1109/toh.2024.3518496.
[15] X. Ma, Y. Qin, L. Zhou, Q. Hu, X. Xiang, H. von Seggern, et al., Fully degradable, highly sensitive pressure sensor based on bipolar electret for biomechanical signal monitoring, Mater. Today Phys., 49(2024). https://doi.org/10.1016/j.mtphys.2024.101597.

[16] X.b. Ji, X.c. Liu, V. Cacucciolo, Y. Civet, A. El Haitami, S. Cantin, et al., Untethered feel-through haptics using 18-μm thick dielectric elastomer actuators, Adv. Funct. Mater., 31(2020) 2006639. https://doi.org/10.1002/adfm.202006639.
[17] M. Park, J.-Y. Yoo, T.y. Yang, Y.H. Jung, A. Vázquez-Guardado, S.p. Li, et al., Skin-integrated systems for power efficient, programmable thermal sensations across large body areas, Proc. Natl. Acad. Sci. U.S.A., 120(2023) e2217828120. https://doi.org/10.1073/pnas.2217828120.
[18] S. Oh, T.-E. Song, M. Mahato, J.-S. Kim, H. Yoo, M.-J. Lee, et al., Easy-to-wear auxetic SMA knot-architecture for spatiotemporal and multimodal haptic feedbacks, Adv. Mater., 35(2023) e2304442. https://doi.org/10.1002/adma.202304442.
[19] M.O. Astam, D. Verheesen, P. Lyu, S.A.M. Weima, D. Liu, Localized and limited-dispersive delivery of thermal stimuli to liquid crystal oligomer networks through radio-frequency media, Adv. Funct. Mater., 34(2024) 2407355. https://doi.org/10.1002/adfm.202407355.
[20] C. Wei, M. Fan, K. Zheng, Multifunctional biomimetic neural tactile sensing system for human-machine interaction, Mater. Today Phys., 57(2025). https://doi.org/10.1016/j.mtphys.2025.101813.
[21] J.T. Su, H. Zhang, H.c. Li, K. He, J.q. Tu, F. Zhang, et al., Skin-inspired multi-modal mechanoreceptors for dynamic haptic exploration, Adv. Mater., 36(2024) e2311549. https://doi.org/10.1002/adma.202311549.
[22] J.M. Qi, F. Gao, G.H. Sun, J.C. Yeo, C.T. Lim, HaptGlove—Untethered pneumatic glove for multimode haptic feedback in reality-virtuality continuum, Adv. Sci., 10(2023) 2301044. https://doi.org/10.1002/advs.202301044.
[23] R. Arbaud, M. Najafi, J.M. Gandarias, M. Lorenzini, U.C. Paul, A. Zych, et al., Toward sustainable haptics: A wearable vibrotactile solar-powered system with biodegradable components, Adv. Mater. Technol., 9(2024) 2301265. https://doi.org/10.1002/admt.202301265.
[24] C. Yiu, Y. Liu, W. Park, J. Li, X. Huang, K. Yao, et al., Skin-interfaced multimodal sensing and tactile feedback system as enhanced human-machine interface for closed-loop drone control, Sci. Adv., 11(2025) eadt6041. https://doi.org/10.1126/sciadv.adt6041.
[25] A. Firouzeh, A. Mizutani, J. Groten, M. Zirkl, H. Shea, PopTouch: A submillimeter thick dynamically reconfigured haptic interface with pressable buttons, Adv. Mater., 36(2023) 2307636. https://doi.org/10.1002/adma.202307636.
[26] S.s. He, J.h. Dai, D. Wan, S. Sun, X. Yang, X. Xia, et al., Biomimetic bimodal haptic perception using triboelectric effect, Sci. Adv., 10(2024) eado6793. https://doi.org/10.1126/sciadv.ado6793.
[27] C. Du Pasquier, L. Tessmer, I. Scholl, L. Tilton, T. Chen, S. Tibbits, et al., Haptiknit: Distributed stiffness knitting for wearable haptics, Sci. Rob., 9(2024) eado3887. https://doi.org/10.1126/scirobotics.ado3887.
[28] R.H. Heisser, C.A. Aubin, O. Peretz, N. Kincaid, H.S. An, E.M. Fisher, et al., Valveless microliter combustion for densely packed arrays of powerful soft actuators, Proc. Natl. Acad. Sci. U.S.A., 118(2021) e2106553118. https://doi.org/10.1073/pnas.2106553118.
[29] B. Lee, H. Cho, K.T. Park, J.-S. Kim, M. Park, H. Kim, et al., High-performance compliant thermoelectric generators with magnetically self-assembled soft heat conductors for self-powered wearable electronics, Nat. Commun., 11(2020) 5948. https://doi.org/10.1038/s41467-020-19756-z.

[30] L.E. Osborn, R. Venkatasubramanian, M. Himmtann, C.W. Moran, J.M. Pierce, P. Gajendiran, et al., Evoking natural thermal perceptions using a thin-film thermoelectric device with high cooling power density and speed, Nat. Biomed. Eng., (2023). https://doi.org/10.1038/s41551-023-01070-w.
[31] Y. Guo, Q.q. Tong, X.z. Liu, X.s. Bian, Z.h. Zhang, Y.r. Zhang, et al., MRS-Tex: A magnetically responsive soft tactile device for texture display, IEEE Trans. Ind. Electron., 69(2022) 11531-40. https://doi.org/10.1109/tie.2021.3120490.
[32] E. Leroy, H. Shea, Hydraulically amplified electrostatic taxels (HAXELs) for full body haptics, Adv. Mater. Technol., 8(2023) 2300242. https://doi.org/10.1002/admt.202300242.
[33] E. Acome, K. Mitchell, T.G. Morrissey, M.B. Emmett, C. Benjamin, M. King, et al., Hydraulically amplified self-healing electrostatic actuators with muscle-like performance, Science, 359(2018) 61-5. https://doi.org/10.1126/science.aao6139.
[34] Q. Xiong, X.Y. Zhou, D.N. Li, J.W. Ambrose, R.C.H. Yeow, An amphibious fully-soft centimeter-scale miniature crawling robot powered by electrohydraulic fluid kinetic energy, Adv. Sci., 11(2024) 2308033. https://doi.org/10.1002/advs.202308033.
[35] F. Hartmann, M. Baskaran, G. Raynaud, M. Benbedda, K. Mulleners, H. Shea, Highly agile flat swimming robot, Sci. Rob., 10(2025) eadr0721. https://doi.org/10.1126/scirobotics.adr0721.
[36] Y. Roh, S. Lee, S.M. Won, S. Hwang, D. Gong, C. Kim, et al., Crumple-recoverable electronics based on plastic to elastic deformation transitions, Nat. Electron., 7(2023) 66-76. https://doi.org/10.1038/s41928-023-01089-6.
[37] X.E. Li, D.N. Rao, M.Q. Zhang, Y.T. Xue, X.N. Cao, S.Y. Yin, et al., A jelly-like artificial muscle for an untethered underwater robot, Cell Rep. Phys. Sci., 5(2024) 101957. https://doi.org/10.1016/j.xcrp.2024.101957.
[38] S.-Y. Jang, M. Cho, H. Kim, M. Choi, S. Mun, J.-H. Youn, et al., Dynamically reconfigurable shape-morphing and tactile display via hydraulically coupled mergeable and splittable PVC gel actuator, Sci. Adv., 10(2024) eadq2024. https://doi.org/10.1126/sciadv.adq2024.
[39] Z.Z. Liu, H. McAleese, A. Weightman, G. Cooper, Optimization of hydraulically amplified electrostatic actuators based on an evolutionary strategy and finite element model to match the performance of the human triceps surae muscle fibres, Extreme Mech. Lett., 63(2023) 102050. https://doi.org/10.1016/j.eml.2023.102050.
[40] B.K. Johnson, M.Naris, V.Sundaram, A. Volchko, K.Ly, S.K.Mitchell, et al., A multifunctional soft robotic shape display with high-speed actuation, sensing, and control, Nat. Commun., 14(2023) 4516. https://doi.org/10.1038/s41467-023-39842-2.
[41] Q.l. Hu, C.j. Jiang, Y. Xie, W. Zhou, L.f. Qin, Y.c. Wang, et al., Rigid electrodes enhance the strain and force output of Peano-HASEL actuators, Appl. Phys. Lett., 123(2023) 254103. https://doi.org/10.1063/5.0174866.
[42] M. Mete, H. Jeong, W.D. Wang, J. Paik, SORI: A softness-rendering interface to unravel the nature of softness perception, Proc. Natl. Acad. Sci. U.S.A., 121(2024) e2314901121. https://doi.org/10.1073/pnas.2314901121.

DSPACE

https://dspace.org/

An ultra-thin and lightweight flexible actuator for digitally-controllable shape-morphing haptics

Chen, Yue; Jiao, Jian; Yu, Xiaobo; Liu, Zhen; Verdin, Patrick G. ...

2026-01-01
Elsevier
https://doi.org/10.1016/j.sna.2025.117233
Chen Y, Jiao J, Yu X, et al., (2026) An ultra-thin and lightweight flexible actuator for digitally-controllable shape-morphing haptics. Sensors and Actuators A: Physical, Volume 397, January 2026, Article number 117233

Downloaded from a DSpace repository. https://dspace.org/